

# Dimensional and Flux Lattice Transitions in Artificially Layered Superconductors

Y. Bruynseraede, K. Temst, E. Osquiguil, C. Van Haesendonck

Laboratorium voor Vaste Stof – Fysika en Magnetisme, Katholieke Universiteit Leuven, B-3001 Leuven, Belgium

A. Gilabert

Laboratoire de Physique de la Matière Condensée, Université de Nice, F-06034 Nice Cedex, France

and

I. K. Schuller

Physics Department 0319, University of California, San Diego, La Jolla, CA 92093-0319, USA

Received January 23, 1992; accepted February 3, 1992

## Abstract

Artificially layered materials are ideal model systems to tune the dimensionality of the superconducting order as well as the structure of the flux line lattice. Our extensive studies of Pb/Ge multilayers indicate that the anisotropy of the upper critical field  $H_{c2}$  strongly depends on the Ge separator thickness  $d_{Ge}$ . The dimensional crossover from  $D = 3$  towards  $D = 2$ , which is revealed by an upturn in the temperature dependence of the parallel critical field  $H_{c2}^{\parallel}$ , is also confirmed by the observed excess fluctuation conductivity above  $T_c$ . In samples for which  $D = 2$  at all temperatures ( $d_{Ge} > 50 \text{ \AA}$ ), the structure of the flux line lattice for a perpendicular field  $H_{\perp}$  can be probed by measuring the critical current density  $J_c$ . The variation of  $J_c(H_{\perp})$  exhibits an anomalous minimum, whose amplitude and position depend on  $d_{Ge}$ , the number of bilayers, temperature, and pinning strength. An interpretation in terms of either flux-lattice decoupling or melting is presented.

## 1. Introduction

The nature of dimensional transitions and the behavior of the flux structure in artificially layered superconductors has been of major interest in recent years, especially in its relation to the properties of high-temperature superconducting oxides [1, 2].

Layered superconductors can be used as model systems to study a variety of physical phenomena including a diversity of dimensional transitions, the interaction between superconductivity and magnetism or electron localization, the enhancement of critical fields and currents [3, 4].

The dimensional transition in superconducting multilayers is closely related to the proximity or electron tunneling coupling between thin superconducting layers across normal or insulating layers. A strong coupling between the superconducting layers occurs when the perpendicular coherence length  $\xi_{\perp}(T)$  is comparable to the multilayer period  $\Lambda$  ( $\Lambda = d_S + d_N$ , with  $d_S$  and  $d_N$  the thickness of the superconducting, resp. normal layer). The divergence of  $\xi_{\perp}$  produces a change from two-dimensional (2D) behavior at low temperatures to three-dimensional (3D) behavior close

to the critical temperature  $T_c$ . This dimensional crossover has been observed in a large number of multilayered systems [5–9].

The observation of dimensional transitions in other physical properties has been restricted to changes in the zero field fluctuation conductivity  $\sigma_{fl}$  as a function of temperature and of fluctuation diamagnetism above  $T_c$  [10, 11]. More recently, the decoupling role of the magnetic field in the 3D to 2D transition in the excess conductivity of layered superconductors was clearly demonstrated [12].

Finally, it has been shown that the magnetic field–temperature ( $H$ – $T$ ) phase diagram of a number of superconductors shows, close to the upper critical field  $H_{c2}(T)$ , a novel phase boundary above which the magnetization of a superconductor is reversible and below which irreversibility sets in [13–20]. Many of the models developed to explain the origin of this phase boundary rely on the layered nature of the superconductor, and deal with a competition between pinning of the vortex lattice in the individual layers or in the multilayered stack. The lower critical field region  $H \simeq H_{c1}$  has been much less investigated up to now. Recent theoretical work [17, 21] has predicted an additional re-entrant vortex fluid phase above  $H_{c1}$ . This low field region of the  $H$ – $T$  diagram has been explored in Pb/Ge multilayers by measuring the critical current density as a function of applied field [22]. Within this context the study of the critical current density  $J_c$  in artificially layered superconductors offers a major advantage over high  $T_c$  superconductors since it is possible to vary almost at will the superconducting layer thicknesses and properties as well as the interlayer coupling.

In this review article we investigate  $H_{c2}(T)$ ,  $\sigma_{fl}(T)$  and  $J_c(T, H)$  of high quality superconducting (Pb) – semiconducting (Ge) multilayers consisting of a varying number of Pb/Ge bilayers. After briefly discussing the preparation and characterization techniques, we first analyze the dimensional transitions observed in the parallel critical field  $H_{c2}^{\parallel}(T)$  and

$\sigma_{fl}(T)$ . This is followed by a report on the unexpected behavior of  $J_c$  as a function of the perpendicular magnetic field. The systematic evolution of this behavior as a function of layer thicknesses, temperature, and pinning strength is related to either flux–lattice decoupling or melting.

## 2. Experimental

### 2.1. Preparation

The Pb/Ge samples were prepared in an UHV chamber equipped with two electron beam guns [23]. The base pressure of the system is  $2 \times 10^{-9}$  Torr, and the pressure did not exceed  $10^{-8}$  Torr during the evaporation. The evaporation rates of the two materials are controlled by a quadrupole mass spectrometer and are respectively 5 Å/s for Pb and 1 Å/s for Ge. In order to ensure a uniform layer growth for the Pb, the samples were evaporated onto liquid nitrogen cooled substrates (oxidized silicon wafers or sapphire). This low substrate temperature leads to an amorphous structure of the Ge films. The layer thicknesses, as monitored with quartz crystals during evaporation, were calibrated using a Dektak profilometer and determined independently by means of the X-ray diffraction spectrum.

Pb is a particularly interesting material to use in the study of the superconducting properties of multilayers. Its low melting point allows an accurate control of the deposition process, while its superconducting properties are rather insensitive to impurities. From the thermodynamic phase diagram it can be concluded that Pb and Ge are immiscible [24], favoring the growth of a highly segregated layered material. The multilayer stack is produced by moving a shutter which alternately interrupts one of the two material beams. Most samples consist of 10 bilayers with a thicker Ge protective capping layer on top. The low-temperature measurements were performed in a standard  $^4\text{He}$  cryostat equipped with a 7 T superconducting coil. The temperature could be varied between 1.5 and 10 K with a stability of a few mK. The critical temperature  $T_c$  and the upper critical field  $H_{c2}$  are determined as the midpoint values of the measured  $R(T)$  and  $R(H)$  transitions. All samples were evaporated onto photolithographically defined lift-off structures containing four lead patterns of  $4.5 \times 0.3 \text{ mm}^2$ . For the structural characterization of the multilayers, extensive X-ray diffraction measurements were performed.

### 2.2. X-ray diffraction

The structure of the samples was investigated by  $\theta$ - $2\theta$  X-ray diffraction experiments on a Rigaku DII Max goniometer equipped with a rotating anode and capable of delivering a maximum power output of 12 kW. A laser system is used to secure an optimal alignment of the sample with respect to the X-ray beam. Data were taken using Cu  $K_\alpha$  radiation with a wavelength  $\lambda = 1.542 \text{ \AA}$ . The diffracted radiation was filtered with a flat pyrolytic monochromator. Because in X-ray diffraction the phase information is lost, real space models have to be developed and their calculated intensities compared with experiment. These structural models have evolved over the last few years from the simple step model to more sophisticated schemes involving various parameters to describe deviations from the ideal superlattice structure. Recently a refinement procedure for fitting the X-ray spectra

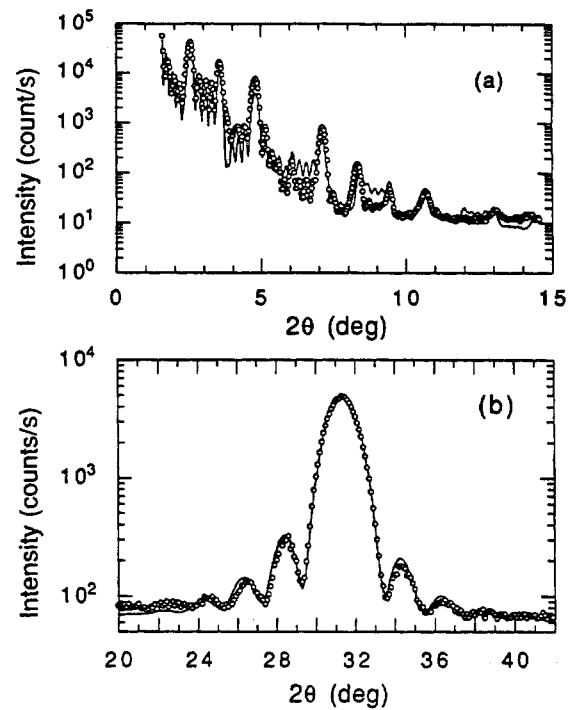


Fig. 1. (a) Experimental (○) and calculated (full line) low angle X-ray diffraction profile of a  $[\text{Pb}(45.4 \text{ \AA})/\text{Ge}(29.5 \text{ \AA})]_5$  superlattice assuming 1 Å of layer thickness fluctuation on both layers. (b) High angle profile of the same superlattice where open circles are the measured intensity and solid line is the refined spectrum

of a wide variety of multilayered structures was developed [25]. This kinematic model takes into account continuous, discrete, and random disorder at the interface and within the layers. A major asset in this calculation scheme is the fact that the structure factor of only one single bilayer needs to be averaged over the variables. Peak positions, relative intensities, and line profiles are then fitted using the non-linear Marquardt algorithm. The resulting optimized values are in excellent agreement with independently obtained results from artificially introduced roughness, EXAFS and XPS studies of the crystal lattice parameters, and determination of the relative thicknesses of the layers by chemical analysis and calibration of sputtering rates [26, 27].

The result of a typical fitting is shown in Fig. 1 for a  $\text{Pb}(45.5 \text{ \AA})/\text{Ge}(29.5 \text{ \AA})$  superlattice. The fitting assumes 1 Å of layer thickness fluctuation on both layers. It can be seen that the fit gives good agreement over several orders of magnitude, both in low and high angle spectra.

## 3. Superconducting Properties

### 3.1. Dimensional transition

3.1.1. *Upper critical field.* Artificially prepared multilayered structures offer an ideal testing ground for the study of physical phenomena operating at different characteristic length scales. In superconductors, the temperature dependent ratio between the layer thickness  $d$  and the coherence length  $\xi$  gives rise to remarkable properties. In particular, the dimensional crossover in the temperature dependence of the parallel critical field was theoretically predicted and experimentally observed in a number of multilayers.

According to the Ginzburg–Landau theory, the upper critical fields parallel and perpendicular to the layers near  $T_c$  of a three dimensional (3D) anisotropic superconductor are

given by

$$H_{c2}^{\parallel} = \frac{\Phi_0}{2\pi\xi_{\parallel}(T)\xi_{\perp}(T)}$$

and

$$H_{c2}^{\perp} = \frac{\Phi_0}{2\pi\xi_{\parallel}(T)^2},$$

where  $\Phi_0$  is the superconducting flux quantum and  $\xi_{\parallel}$  and  $\xi_{\perp}$  are the superconducting coherence lengths parallel and perpendicular to the layers. Taking into account that the coherence length diverges near the critical temperature  $T_c$  as  $(T_c - T)^{-1/2}$ , we find a linear temperature dependence for both  $H_{c2}^{\parallel}$  and  $H_{c2}^{\perp}$  in 3D.

If there is no superconducting coupling between the layers, the critical field of a stack of independent thin superconducting slabs is observed. A superconducting film is two dimensional (2D) when its thickness  $d_s < \xi(T=0)$  in the bulk material. For multilayers this unperturbed coherence length corresponds to the coherence length  $\xi_{\parallel}$  in the plane of the superconducting layer. Tinkham calculated the parallel critical field for a thin superconducting slab of thickness  $d_s \ll \xi_{\parallel}$

$$H_{c2}^{\parallel}(T) = \frac{\Phi_0 \sqrt{12}}{2\pi\xi_{\parallel}(T)d_s},$$

which leads to a square-root temperature dependence of  $H_{c2}^{\parallel}$  in 2D.

The perpendicular coherence length  $\xi_{\perp}$  is a measure of the coupling strength. If the thickness of the separator layer is suitably chosen, the sample can change from uncoupled to coupled behavior as  $\xi_{\perp}$  increases with increasing temperature. When  $\xi_{\perp}(T)$  becomes comparable to the separator thickness  $d_{Ge}$ , superconducting coupling between the layers is established. This phenomenon, denoted as the “2D–3D dimensional crossover”, has been observed earlier in a variety of multilayered systems and can be readily investigated through the temperature dependence of the parallel critical field  $H_{c2}^{\parallel}$ .

### 2D–3D transitions

We will illustrate the dimensional crossover in a set of Pb/Ge samples having different Ge thicknesses [8, 28]. The critical fields of these multilayers are shown in Fig. 2. A square-root temperature dependence of  $H_{c2}^{\parallel}$  at all temperatures is observed for Pb/Ge systems with  $d_{Ge} > 30 \text{ \AA}$ . This indicates that the Pb layers are uncoupled and that the individual Pb layers are 2D. As the Ge thickness is decreased to  $20 \text{ \AA}$ , a dimensional crossover occurs. Because  $\xi_{\perp}$  is large close to  $T_c$ , the Pb layers are coupled. The sample is then 3D, which is reflected by the linear temperature dependence of  $H_{c2}^{\parallel}$ . As the temperature is lowered,  $\xi_{\perp}$  is reduced. When  $\xi_{\perp} < d_{Ge}$  the magnetic flux is confined to the Ge layers, inducing a decoupling of the 2D superconducting slabs. The decoupling is reflected by a pronounced upturn of  $H_{c2}^{\parallel}$ . Finally, a sample with only  $15 \text{ \AA}$  Ge shows a coupled 3D behavior, reflected in the linear temperature dependence of  $H_{c2}^{\parallel}(T)$ .

Also indicated in this graph are the perpendicular critical fields of these multilayers. In all cases the perpendicular critical field has a linear temperature dependence. Since  $H_{c2}^{\perp}$  only probes the parallel coherence length  $\xi_{\parallel}$ , it does not

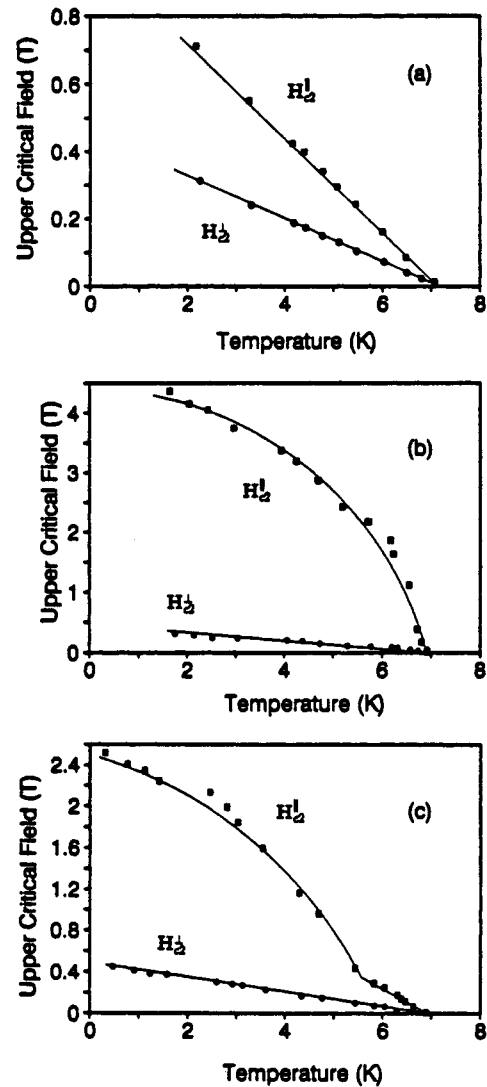


Fig. 2. Parallel (■) and perpendicular (●) critical fields for Pb/Ge multilayers with (a)  $140 \text{ \AA}$  Pb and  $15 \text{ \AA}$  Ge, (b)  $140 \text{ \AA}$  Pb and  $42 \text{ \AA}$  Ge, and (c)  $140 \text{ \AA}$  Pb and  $20 \text{ \AA}$  Ge. In (c) the dimensional crossover occurs at the upturn in the parallel critical field. The solid lines are a guide to the eye

offer any information on the dimensionality of the whole multilayer system. It does allow however to calculate  $\xi_{\parallel}$  from the measured value of  $H_{c2}^{\perp}$ . The resulting  $\xi_{\parallel}(T \rightarrow 0) \approx 280 \text{ \AA}$  is larger than the Pb layer thickness  $d_{Pb} = 140 \text{ \AA}$ , justifying the treatment of the individual Pb layers as 2D slabs.

### 2D–2D transitions

The ability to fine tune the coupling can further be demonstrated by means of the so-called “2D–2D” crossover [9]. For these experiments several sets of samples were produced containing only two Pb layers, in a Ge/Pb/Ge/Pb/Ge sequence. Within each set the Pb thickness was kept constant (resp.  $70 \text{ \AA}$ ,  $80 \text{ \AA}$  and  $140 \text{ \AA}$ ) while the thickness of the separating Ge layer was varied between  $5 \text{ \AA}$  and  $40 \text{ \AA}$ . The top Ge layer was always  $500 \text{ \AA}$ . The Pb layers were evaporated simultaneously for all samples in one set, in order to rule out spurious changes in structure, composition, film thickness, etc., which may influence  $T_c$ . The different Ge thicknesses are obtained by moving a shutter across the substrate during evaporation.

Figure 3 shows the upper critical fields parallel and perpendicular to the layers as a function of the reduced temperature  $T/T_c$  for the set of samples with  $d_{Pb} = 70 \text{ \AA}$  and

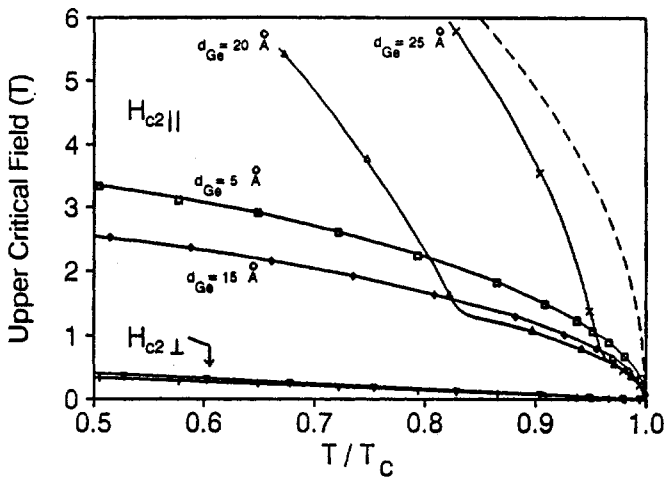


Fig. 3. Parallel critical field for four samples from the  $d_{\text{Pb}} = 70 \text{ \AA}$  multilayer set with different Ge thicknesses [ $5 \text{ \AA}$  ( $\square$ );  $15 \text{ \AA}$  ( $\diamond$ );  $20 \text{ \AA}$  ( $\Delta$ );  $25 \text{ \AA}$  ( $\times$ )]. The perpendicular critical field  $H_{c2}^{\perp}$  is shown for the  $d_{\text{Ge}} = 5 \text{ \AA}$  sample ( $+$ ) and the  $d_{\text{Ge}} = 25 \text{ \AA}$  sample ( $\nabla$ ). The dashed line represents the parallel critical field of a  $70 \text{ \AA}$  single Pb film sandwiched between thick Ge. The solid lines are a guide to the eye. The 2D-2D crossover is clearly seen in the samples with  $d_{\text{Ge}} = 20 \text{ \AA}$  and  $d_{\text{Ge}} = 25 \text{ \AA}$

different  $d_{\text{Ge}}$ . The temperature dependence of  $H_{c2}^{\perp}$  is linear as expected and does not change appreciably with Ge thickness. From the perpendicular critical fields a parallel coherence length  $\xi_{\parallel}(T \rightarrow 0) \simeq 220 \text{ \AA}$  was determined for all samples.

Since  $\xi_{\parallel} > d_{\text{Pb}}$ , the individual films are 2D at all temperatures. But since  $\xi_{\parallel}$  is also larger than the sum of the two Pb/Ge bilayer thicknesses ( $\xi_{\parallel} > 2\lambda$ ), we expect a 2D behavior for the coupled multilayer as well (provided  $\xi_{\perp} > d_{\text{Ge}}$ ). As shown in Fig. 3,  $H_{c2}^{\parallel} \propto (T_c - T)^{1/2}$  for the multilayer with  $d_{\text{Ge}} = 5 \text{ \AA}$ . The amplitude of  $H_{c2}^{\parallel}(T)$  coincides exactly with the measured critical field of a  $140 \text{ \AA}$  single Pb film, sandwiched between Ge (not shown). From Tinkham's formula the effective superconducting layer thickness  $d_{\text{Pb}}^{\text{eff}} \simeq 130 \text{ \AA}$ , indicating that the two Pb layers are coupled through the Ge layer. Since  $2\lambda$  is smaller than  $\xi_{\parallel}(0)$ , the coupled multilayer behaves as a 2D superconductor.

Increasing the Ge thickness initially leads to a decrease of  $H_{c2}^{\parallel}$  for  $d_{\text{Ge}} = 15 \text{ \AA}$ , until for  $d_{\text{Ge}} = 20 \text{ \AA}$  a remarkable upturn of  $H_{c2}^{\parallel}$  occurs at lower temperature. This jump corresponds to a crossover from the 2D coupled multilayer close to  $T_c$ , towards the state of two decoupled 2D Pb films at lower temperatures. It is therefore important to note that  $H_{c2}^{\parallel}$  of the  $d_{\text{Ge}} = 20 \text{ \AA}$  and  $d_{\text{Ge}} = 25 \text{ \AA}$  multilayers has a 2D non-linear temperature dependence below as well as above the crossover temperature. A further increase of  $d_{\text{Ge}}$  shifts the critical field towards the  $H_{c2}^{\parallel}$  value of a  $70 \text{ \AA}$  Pb film sandwiched between two Ge layers (dashed line). Qualitatively the same results were obtained in the set of samples with  $d_{\text{Pb}} = 140 \text{ \AA}$ .

The decoupling process can be seen in detail in Fig. 4 where measurements of the resistive transition at fixed temperatures are presented for a similar multilayer with  $d_{\text{Pb}} = 80 \text{ \AA}$  and  $d_{\text{Ge}} = 25 \text{ \AA}$ . The resistance of the multilayer is plotted as a function of parallel magnetic field for several values of  $T/T_c$ . When  $T/T_c = 0.985$ , the transition of the coupled multilayer is sharp and is comparable to the resistive transition of a  $160 \text{ \AA}$  single Pb film. For  $T/T_c = 0.971$  and  $0.966$ , the 2D-2D crossover manifests itself by a

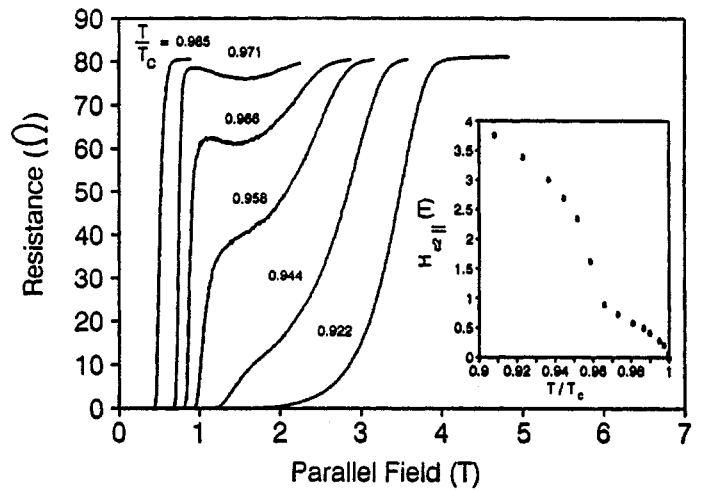


Fig. 4. Resistance vs. parallel magnetic field of a Pb( $80 \text{ \AA}$ )/Ge( $25 \text{ \AA}$ ) multilayer consisting of two bilayers, for several values of  $T/T_c$ . The 2D-2D crossover is seen by a decrease of the multilayer resistance with increasing field. The inset shows  $H_{c2}^{\parallel}$  as a function of reduced temperature, determined by the midpoint values of the resistive transition

decrease of the resistance with increasing parallel magnetic field. This drop in the resistance is caused by a sudden increase of  $H_{c2}^{\parallel}$  when the Pb layers get decoupled. At still lower temperatures ( $T/T_c < 0.944$ ), the transition is identical to that of a  $80 \text{ \AA}$  single Pb film, sandwiched between Ge. These  $R(H_{\parallel})$  measurements stress the importance of the parallel magnetic field in the decoupling process.

Two theoretical models provide the background for these coupling/decoupling experiments. In the Klemm, Luther, and Beasley model [29] the interlayer coupling is dominated by the Josephson effect. The coupling strength is described by the coupling parameter  $r = (J^2\tau)/k_B T_c \hbar$  where  $J$  is the Josephson coupling energy and  $\tau$  the electron lifetime due to disorder. When this coupling parameter  $r$  is equal to zero, the layers are decoupled. For  $r > 0$  the system can be coupled or may show a crossover. The critical field data for the Nb( $65 \text{ \AA}$ )/Ge( $35 \text{ \AA}$ ) system, in which a dimensional crossover was observed [5], were fitted to this theory, leading to a coupling parameter  $r = 0.1$ .

Tachiki and Takahashi on the other hand have calculated the critical fields of proximity coupled systems [30]. The three important parameters in their model are the ratio of the density of states, of the electronic diffusion coefficients, and of the BCS interaction constants. These quantities are assumed to be constant within one layer and to change discontinuously at the interface. The dimensional crossover turns up as a consequence of the difference in the density of states, while taking in each layer equal values for the other two parameters. Their model has proved to be successful to fit data of Nb/Cu [6], a proximity coupled system in which a crossover occurs. For superconductor/insulator ( $N_N/N_S = 0$ ) multilayers, the theory predicts the 2D square root dependence of  $H_{c2}^{\parallel}(T)$  as is observed in Pb/Ge multilayers with  $d_{\text{Ge}} > 30 \text{ \AA}$ . However in multilayers with  $d_{\text{Ge}} < 30 \text{ \AA}$  the temperature at which the dimensional crossover occurs, corresponds to a value  $N_N/N_S \simeq 0.05$ . This finite value for the density of states in Ge may be due to the creation of defect states within the bandgap near the Ge/Pb interface.

3.1.2. *Superconducting fluctuations.* The dimensionality of the system also manifests itself in fluctuation effects. The influence of thermodynamic fluctuations is more important

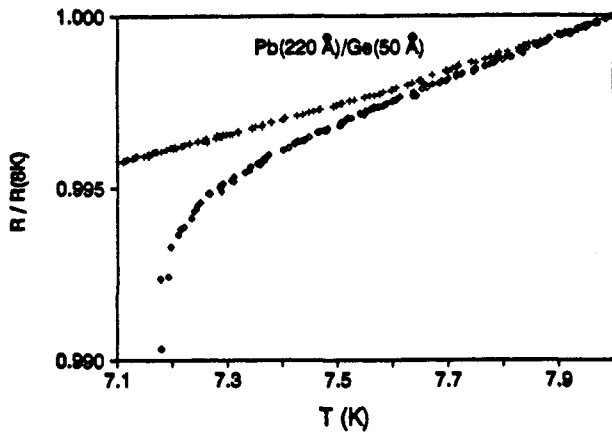


Fig. 5. Zero field resistive transition of the Pb(220 Å)/Ge(50 Å) multilayer ( $\diamond$ ), compared with the normal-state resistance, measured in a 1 T perpendicular field ( $+$ )

in systems with reduced dimensionality. We have performed detailed measurements of the excess conductivity above the critical temperature in Pb/Ge multilayers [12]. The amplitude and temperature dependence of these fluctuations yield information on the dimensionality of the system.

In the Ginzburg–Landau approximation the excess conductivity  $\sigma_{fl}$  for bulk materials is calculated by Aslamazov and Larkin [31, 32] as

$$\sigma_{fl}^{3D} = \frac{e^2}{32\hbar\xi(0)} \varepsilon^{-1/2},$$

where  $\varepsilon = (T/T_c - 1)$ .

For a two-dimensional film with thickness  $d$  we find

$$\sigma_{fl}^{2D} = \frac{e^2}{16\hbar d} \varepsilon^{-1}.$$

Figure 5 shows the resistive transition of a Pb(220 Å)/Ge(50 Å) multilayer in zero field and the normal state resistance *vs.* temperature measured in a perpendicular field of 1 T (which is higher than the perpendicular critical field in the measured temperature range). The resistance has been normalized to its value at 8 K. The presence of an excess fluctuation conductivity in zero field below 8 K is clear from this graph. Plotting  $\ln \sigma_{fl}$  *vs.*  $\ln \varepsilon$  yields a slope equal to  $-1$  (Fig. 6), indicating that the sample is 2D. This is corroborated by our measurements of the parallel critical

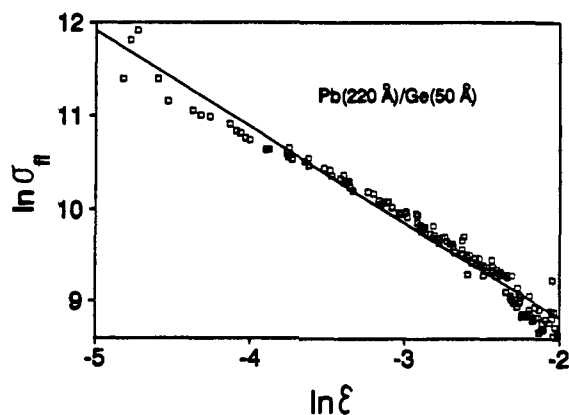


Fig. 6. Logarithmic plot of the excess conductivity *vs.* temperature ( $\square$ ) for the Pb(220 Å)/Ge(50 Å) multilayer of Fig. 5. A least squares fit (solid line) yields  $\ln \sigma_{fl} = 6.76 - 1.03 \ln \varepsilon$ , confirming the 2D nature of the fluctuation conductivity

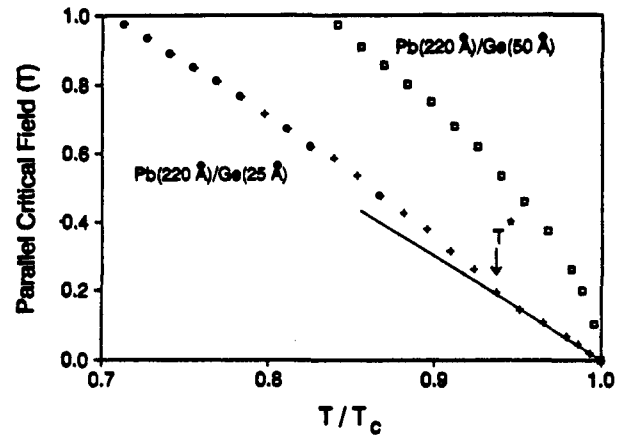


Fig. 7. Parallel critical field *vs.* reduced temperature for a Pb(220 Å)/Ge(25 Å) ( $+$ ) and a Pb(220 Å)/Ge(50 Å) ( $\square$ ) multilayer. The solid line emphasizes the linear temperature dependence of  $H_{c2}^{\parallel}$  close to  $T_c$  of the Pb(220 Å)/Ge(25 Å) multilayer.  $T^*$  indicates the crossover temperature

field, which show the typical square-root temperature dependence. It was found that the Maki–Thompson correction term can be neglected because of the strong pair-breaking in Pb [33, 34].

The situation is different for a Pb(220 Å)/Ge(25 Å) multilayer. This sample has a dimensional crossover in the parallel critical field, as shown in Fig. 7. The resistive transition from the superconducting to the normal state in the presence of a parallel magnetic field will therefore have a 2D or 3D character depending on its location in the  $H$ – $T$  diagram. If the transition point is in the 3D linear region (above  $T^*$ ), we expect 3D superconducting fluctuations to occur. However in the 2D parabolic part of the phase boundary, we expect 2D fluctuations. A parallel magnetic field allows us to move along the phase boundary.

We therefore compare in Fig. 8 the resistive transition in an applied magnetic field  $H_{\parallel} = 0.07$  T and  $H_{\parallel} = 0.8$  T with the normal-state resistance, measured in a 1 T perpendicular field. For the lower field  $H_{\parallel} = 0.07$  T the sample is in the 3D part of the  $H$ – $T$  phase diagram, while for  $H_{\parallel} = 0.8$  T the transition point shifts to the 2D part. In the latter case we see that the resistive transition is more rounded, already indicating the appearance of 2D fluctuations. This can be seen more quantitatively in Fig. 9 where  $\ln \sigma_{fl}$  *vs.*  $\ln \varepsilon$  is

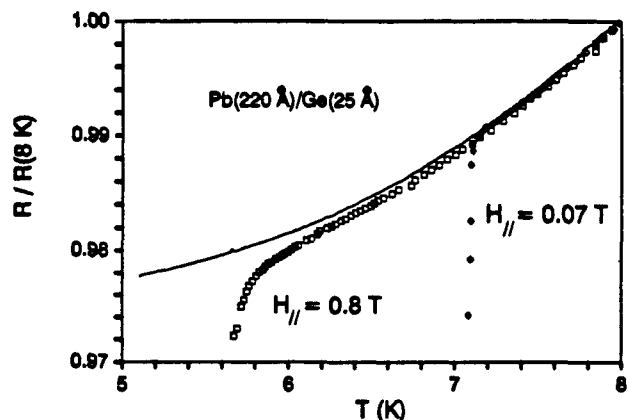


Fig. 8. Resistive transition of the Pb(220 Å)/Ge(25 Å) multilayer in the 3D region [with  $H_{\parallel} = 0.07$  T ( $\diamond$ )], and in the 2D region [with  $H_{\parallel} = 0.8$  T ( $\square$ )]. The solid line is the normal-state resistance, measured in a 1 T perpendicular field

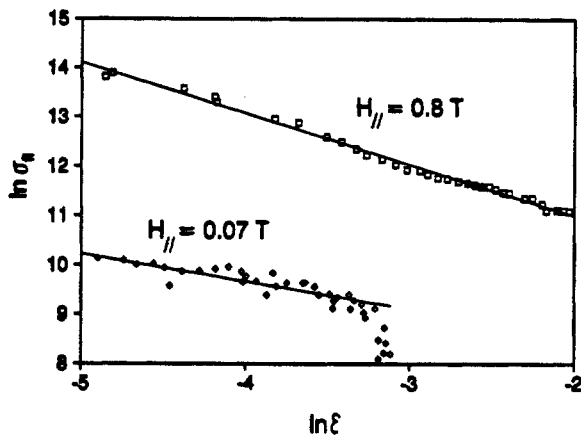


Fig. 9. Logarithmic plot of the excess conductivity vs. temperature for the Pb(220 Å)/Ge(25 Å) multilayer, shown in Fig. 8. The solid lines are linear fits to the data

plotted for the two field values. A linear fit to the data yields a slope of  $-0.47$  for  $H_{||} = 0.07$  T and  $-1.09$  when  $H_{||} = 0.8$  T. The change in slope from about  $-1/2$  to  $-1$  when applying a larger magnetic field clearly indicates a change in dimensionality, thus confirming the results of the parallel critical field experiments.

### 3.2. Flux lattice transition

Apart from the above mentioned experiments which study the superconducting coupling in these multilayers the flux line lattice coupling was investigated as well. To pursue this goal the critical current in Pb/Ge multilayers as a function of applied field was measured.

Tachiki and Takahashi theoretically considered the pinning in a layered structure as a function of the angle between the applied field and the layers [35]. They showed that the pinning reaches a maximum when the field is applied parallel to the layers, while the pinning is at its lowest value for the perpendicular orientation. This was confirmed experimentally by measuring the angular dependence of the critical current in  $\text{YBa}_2\text{Cu}_3\text{O}_7$  crystals [36]. Figure 10 shows the critical current as a function of the angle of a Pb/Ge multilayer consisting of 10 bilayers with 220 Å Pb and 50 Å Ge at 4.2 K in a fixed field of 0.1 Tesla. From the measured I-V curves,  $J_c$  was determined using a  $4.4 \mu\text{V}/\text{cm}$  criterion and the total Pb cross sectional area of the multilayer. A qualitative agreement with the theoretical

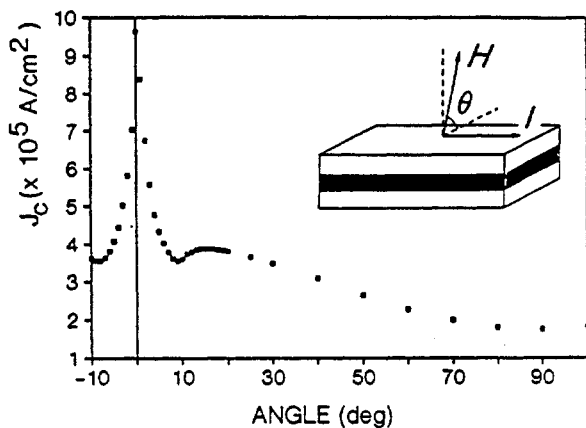


Fig. 10. Critical current density at 4.2 K for a Pb(220 Å)/Ge(50 Å) multilayer as a function of the angle between an applied magnetic field of 0.1 T and the layers. The inset shows the geometrical configuration

prediction is found, i.e. the pinning strength and hence the critical current reach a maximum when the field is parallel to the layers, caused by the enhanced pinning at the Ge layers. Furthermore, the critical current reaches its lowest value when the field is perpendicular to the layers. There is however an unexpected feature in the angular dependence of  $J_c$ . Near  $\theta = 10^\circ$  there is a well pronounced minimum, followed by a broader maximum before  $J_c$  finally decreases monotonically to zero at  $H_{c2}$ .

In order to investigate the origin of this extra minimum, the sample was measured in various applied fields. Figure 11 shows that the position of the minimum shifts to smaller angles as the field is increased and the minimum always occurs for the same perpendicular component of the field, i.e.  $H_{\perp} = H \sin \theta_{\min}$  remains constant. Therefore attention was focused on the perpendicular field component and all further experiments were performed in a field exactly perpendicular to the layers.

Figure 12 shows the resistively measured  $J_c$  at  $T = 4.2$  K for a single Pb film [i.e. a Ge(60 Å)/Pb(140 Å)/Ge(500 Å) sandwich] and for two multilayers with 140 Å Pb and 60 Å Ge and with 5 and 10 bilayers respectively. The  $J_c$  data show that the minimum is more pronounced as the number of bilayers is increased and that the field  $H_{\perp}^*$  where the minimum occurs shifts with the number of bilayers.

The effect is also dependent on the thickness of the Ge layer as shown in Fig. 13. The critical current densities at 5 K for a single film (thickness 250 Å) and three multilayers with 50 bilayers of 200 Å Pb but varying Ge thickness were extracted from the magnetic hysteresis loops using Bean's model. Because of uncertainties in the sample volume and the demagnetization factor the data were normalized with respect to the zero field value. The  $J_c$  of the multilayer with

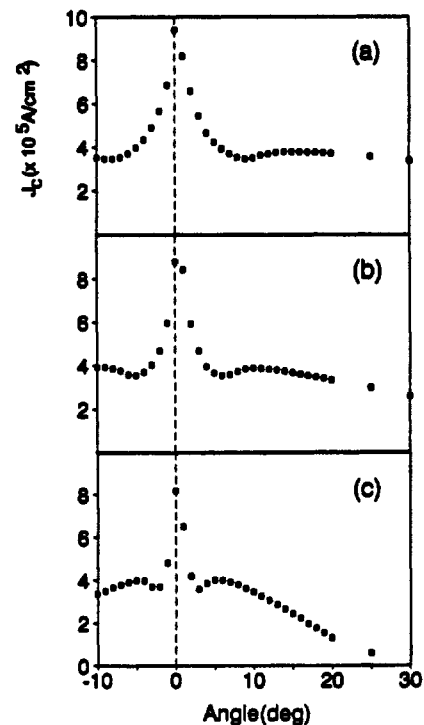


Fig. 11. Critical current density at 4.2 K for a Pb(220 Å)/Ge(50 Å) multilayer as a function of the angle and at different magnetic fields. In (a)  $H = 0.1$  T and  $\theta_{\min} = 9^\circ$ , in (b)  $H = 0.15$  T and  $\theta_{\min} = 6^\circ$ , and in (c)  $H = 0.3$  T and  $\theta_{\min} = 3^\circ$ . The perpendicular component  $H_{\perp} = H \cdot \sin \theta_{\min}$  remains constant

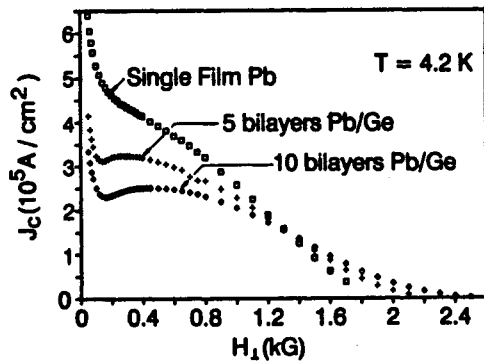


Fig. 12. Critical current density  $J_c$  at 4.2 K for a single Pb film and two Pb(140 Å)/Ge(60 Å) multilayers with a different number of bilayers

$d_{Ge} = 20 \text{ \AA}$  drops much faster than that of the single film. For the multilayers with  $d_{Ge}$  equal to 50 Å and 200 Å the minimum appears and, as the field is increased,  $J_c$  coincides with that of the single film. The transition field  $H_{\perp}^*$  from multilayer to single film-like behavior moves to higher fields when  $d_{Ge}$  decreases.

The field  $H_{\perp}^*$  is not only thickness- but also temperature-dependent as shown in Fig. 14, where  $J_c$ , obtained from transport measurements and normalized by  $J_c(50 \text{ G})$ , is plotted as a function of  $H_{\perp}$  for a multilayer consisting of 10

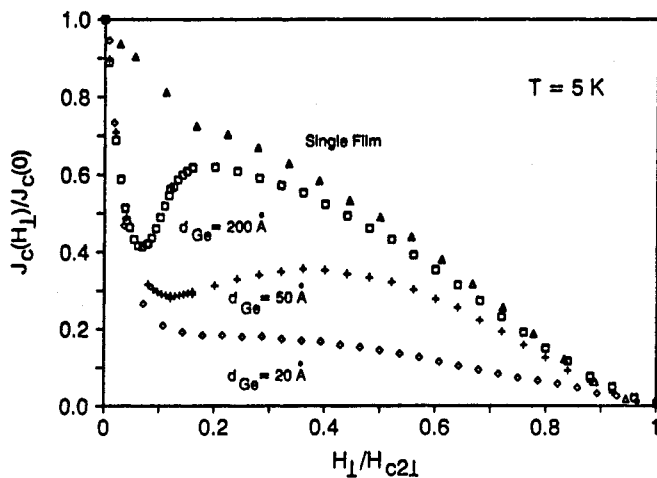


Fig. 13. Normalized critical current densities vs.  $H_{\perp}/H_{c2\perp}$ , determined from magnetization measurements, for a single Pb film and for three Pb/Ge multilayers with  $d_{Pb} = 200 \text{ \AA}$  but different  $d_{Ge}$  [ $d_{Ge} = 200 \text{ \AA}$  ( $\square$ ),  $d_{Ge} = 50 \text{ \AA}$  ( $+$ ), and  $d_{Ge} = 20 \text{ \AA}$  ( $\diamond$ )]

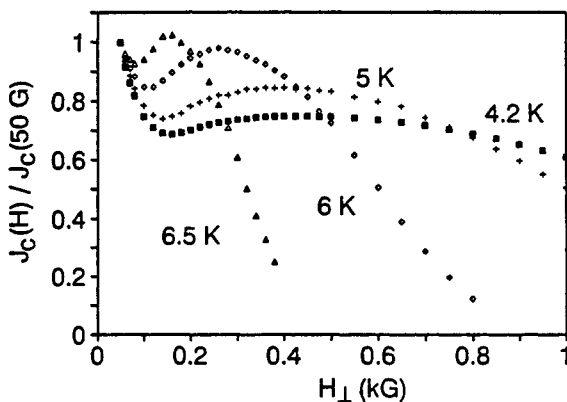


Fig. 14. Normalized critical current densities vs.  $H_{\perp}$  for a Pb(140 Å)/Ge(60 Å) multilayer with 10 bilayers at different temperatures. The shift of the minimum when the temperature is varied, excludes matching effects as the origin for this minimum

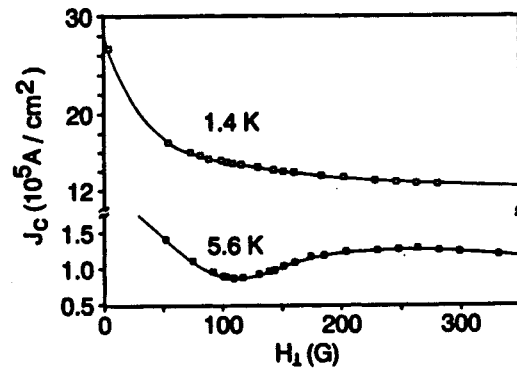


Fig. 15. Critical current density vs.  $H_{\perp}$  for a Pb(140 Å)/Ge(50 Å) multilayer with 50 bilayers, showing that the minimum disappears at low temperatures

bilayers, each with 140 Å Pb and 60 Å Ge. The fact that the position of the minimum is temperature dependent excludes matching effects as a possible explanation for this phenomenon.

At sufficiently low temperatures  $J_c(H_{\perp})$  reverts to a monotonically decreasing behavior, while the same sample has a clear cut minimum at 5.6 K as is illustrated in Fig. 15 for a [Pb(140 Å)/Ge(50 Å)]<sub>5</sub> multilayer.

The role of pinning was investigated by doping the Pb layers with Bi. Figure 16 shows  $J_c(H_{\perp})$  for a [Pb(100 Å)/Ge(50 Å)]<sub>10</sub> and a [Pb<sub>0.85</sub>Bi<sub>0.15</sub>(100 Å)/Ge(50 Å)]<sub>10</sub> multilayer. The addition of Bi to the Pb layers raises the critical current density and suppresses the presence of the minimum.

The fact that both a lowering of the temperature and the increase of the pinning strength lead to disappearance of the minimum implies that thermal fluctuations play a crucial role. The minimum in  $J_c(H_{\perp})$  may therefore be interpreted as a thermally driven softening of the flux line lattice. The vortex lattice undergoes a structural transition at  $H_{\perp}^*$ . Two different theoretical approaches have been advanced that could explain this softening. The first is the magnetic decoupling mechanism proposed by Clem [37–39], which is closely related to the behavior of the flux line lattice in a superconducting transformer. The basic idea is sketched in Fig. 17 [40]. At low fields there is a rigid vortex lattice. As the field is increased, the vortices are sitting closer one to another, leading to a nearly homogeneous field distribution in the non-superconducting Ge layers. This effectively leads to a decoupling of the vortex lattice from layer to layer,

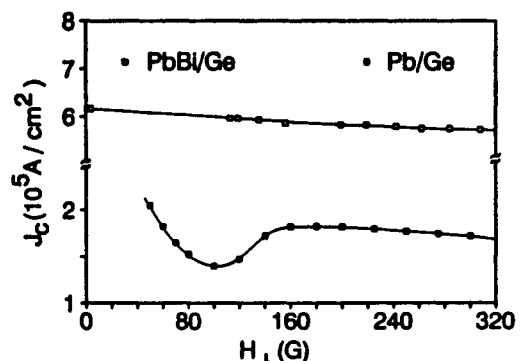


Fig. 16. Comparison between  $J_c(H_{\perp})$  for a Pb(100 Å)/Ge(50 Å) multilayer and a Pb<sub>0.85</sub>Bi<sub>0.15</sub>(100 Å)/Ge(50 Å) multilayer, both having 10 bilayers

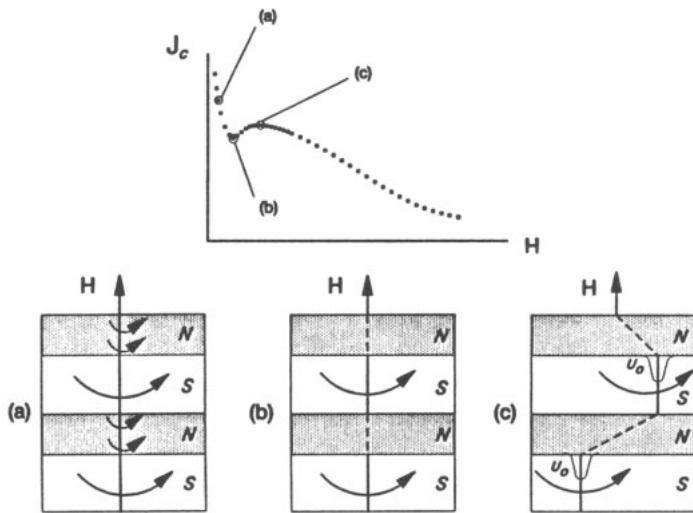


Fig. 17. Scheme to illustrate the  $J_c(H_{\perp})$  behaviour in terms of the magnetic decoupling model. In (a) there is a rigid vortex lattice. In (b) there is a nearly homogeneous field distribution in the normal layers, due to the increasing flux, leading to a decoupling of the flux lines from one superconducting layer to the other. Finally, in (c) the flux lines rearrange themselves within the superconducting layers to take advantage of the available pinning centers (indicated by potential wells  $U_0$ ).

leaving a system of stacked 2D pancake vortex lattices in each Pb layer. The vortices can rearrange themselves within each layer to take advantage of the available pinning centers, thus increasing the critical current. This is indicated on the graph by the vortices which are “trapped” in pinning potential wells  $U_0$ .

The other plausible explanation is a melting of the initially 3D vortex lattice. This melting is due to an exponential decay of the vortex-vortex interaction at low fields such that the flux line lattice is very sensitive to thermal fluctuations. When pinning can be neglected, this causes the presence of a field regime above  $H_{c1}^{\perp}$  where  $J_c$  should be zero, while  $J_c$  increases again at higher fields. For sufficiently strong pinning this melting transition is suppressed. It can be expected that for intermediate pinning strengths  $J_c$  should develop a minimum instead of dropping completely to zero. The field  $H_{\perp}^*$  is plotted in the  $H_{\perp}$ - $T$  diagram in Fig. 18. Within the melting model, a qualitatively similar behavior for the low-field phase boundary has been predicted for

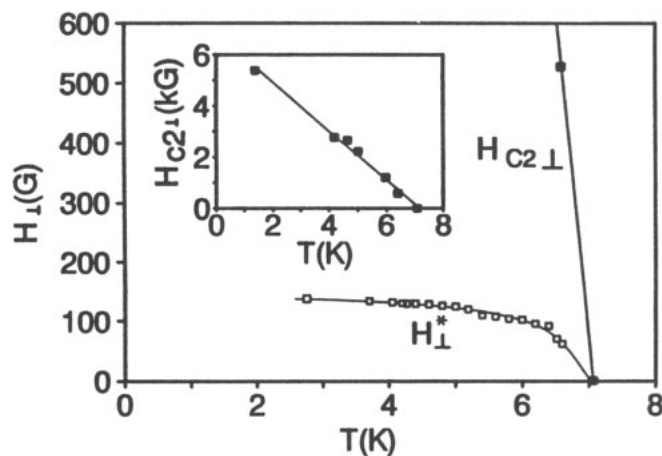


Fig. 18.  $(H_{\perp}, T)$  phase diagram of Pb/Ge multilayers. The open squares represent the field  $H_{\perp}^*$  (the solid line is a guide to the eye) while the solid squares correspond to the upper critical field  $H_{c2}^{\perp}$ . The inset shows the linear temperature dependence of  $H_{c2}^{\perp}$  over the whole temperature range

weak pinning [21]. Further experiments are being performed to elucidate the exact mechanism responsible for the observed  $J_c(H_{\perp})$  behavior.

#### 4. Conclusions

Artificially layered superconductors are ideal systems for studying thin film-, dimensional-, proximity-, coupling- and superlattice effects. These parameters can be well controlled, enabling a finetuning of the material properties and the creation of novel structures which do not occur naturally. As a consequence they are also useful as model systems to evaluate theoretical models related to the physics of dimensionality and phase transitions.

In this review we explored dimensional transitions using critical magnetic field and excess conductivity data as well as the analysis of transitions in the magnetic field-temperature phase diagram using critical current data.

In conclusion, the advent of high temperature superconductivity in ceramic oxides opened new perspectives for artificially layered superconductors to be used as testing systems to distinguish properties which are a consequence of the layered nature and others which are due to more exotic and yet unknown phenomena.

#### Acknowledgements

This work has been supported by the Belgian High Temperature Superconductor Impulse Program No. SU/01/001 and the Concerted Actions Programs No. 88/93-130 at KUL and the Office of Naval Research Grant No. N00014-88-K-0480 at UCSD. International travel was provided by NATO. K.T. is a Research Fellow of the Belgian I.I.K.W. and C.V.H. is a Senior Research Associate of the Belgian N.F.W.O. We thank V. V. Moshchalkov, J. Clem, D. Bishop, J. Guimpel, A. Kapitulnik and L. Glazman for useful conversations.

#### References

1. For a review see for instance Beasley, M. R., in “Synthetic Modulated Structures”, (Edited by L. L. Chang and B. C. Giessen) (Academic Press, New York, 1985), p. 365.
2. For a recent review see for instance Schuller, I. K., Guimpel, J. and Bruynseraede, Y., Mater. Res. Bull. **25**, 29 (1990).
3. Schuller, I. K., in “Physics, Fabrication and Applications of Multilayered Structures, (Edited by P. Dhez and C. Weisbuch, (Plenum Press, New York, 1988), p. 139.
4. For a recent review see Jin, B. Y. and Ketterson, J. B., Adv. Phys. **38**, 189 (1989).
5. Ruggiero, S. T., Barbee, T. W. Jr. and Beasley, M. R., Phys. Rev. **B26**, 4894 (1982).
6. Banerjee, I., Yang, Q. S., Falco, C. M. and Schuller, I. K., Phys. Rev. **B28**, 5037 (1983).
7. Kanoda, K., Mazaki, H., Yamada, T., Hosoito, N. and Shinjo, T., Phys. Rev. **B33**, 2052 (1986).
8. Neerinck, D., Temst, K., Vanderstraeten, H., Van Haesendonck, C., Bruynseraede, Y., Gilabert, A. and Schuller, I. K., J. Phys.: Condens. Matter **2**, 6287 (1990).
9. Neerinck, D., Temst, K., Van Haesendonck, C., Bruynseraede, Y., Gilabert, A. and Schuller, I. K., Phys. Rev. **B43**, 8676 (1991).
10. Ruggiero, S. T., Barbee, T. W., Jr. and Beasley, M. R., Phys. Rev. Lett. **45**, 1299 (1980).
11. Obara, H., Uchinokura, K. and Tanaka, S., Jpn. J. Appl. Phys. **26**, 1437 (1987).
12. Neerinck, D., Temst, K., Van Haesendonck, C., Bruynseraede, Y., Gilabert, A. and Schuller, I. K., Europhys. Lett. **15**, 637 (1991).
13. Müller, K. A., Takashige, M. and Bednorz, J. G., Phys. Rev. Lett. **58**, 1143 (1987).
14. Yeshurun, Y. and Malozemoff, A. P., Phys. Rev. Lett. **60**, 2202 (1988).

15. Guimpel, J., Høghøj, P., Schuller, I. K., Vanacken, J. and Bruynseraede, Y., *Physica C* **175**, 197 (1991).
16. Gammel, P. L., Schneemeyer, L. F., Waszczak, J. V. and Bishop, D. J., *Phys. Rev. Lett.* **61**, 1666 (1988).
17. Nelson, D. R., *Phys. Rev. Lett.* **60**, 1973 (1988).
18. Brandt, E. H., *Phys. Rev. Lett.* **63**, 1106 (1989).
19. Clem, J. R., *Phys. Rev.* **B43**, 7837 (1991).
20. Glazman, L. I. and Koshelev, A. E., *Phys. Rev.* **B43**, 2835 (1991).
21. Fisher, D. S., Fisher, M. P. A. and Huse, D. A., *Phys. Rev.* **B43**, 130 (1991).
22. Neerincx, D., Temst, K., Baert, M., Osquiguil, E., Van Haesendonck, C., Bruynseraede, Y., Gilabert, A. and Schuller, I. K., *Phys. Rev. Lett.* **67**, 2577 (1991).
23. Sevenhans, W., Locquet, J. P. and Bruynseraede, Y., *Rev. Sci. Instrum.* **57**, 937 (1986).
24. Lupis, C. H. P., in "Classical Thermodynamics of Materials", (North-Holland, New York, 1983).
25. Schuller, I. K., Fullerton, E. E., Vanderstraeten, H. and Bruynseraede, Y., *Mat. Res. Soc. Symp. Proc.* Vol. 229, 41 (1991).
26. Fullerton, E. E., Schuller, I. K., Vanderstraeten, H. and Bruynseraede, Y., submitted to *Phys. Rev. B*.
27. The SUPREX refinement program is IBM PC compatible and is available from the authors (Y.B. and I.K.S.)
28. Locquet, J. P., Neerincx, D., Vanderstraeten, H., Sevenhans, W., Van Haesendonck, C., Bruynseraede, Y., Homma, H. and Schuller, I. K., *Japan J. Appl. Phys.* **26**, 1431, (1987).
29. Klemm, R. A., Luther, A. and Beasley, M. R., *Phys. Rev.* **B12**, 877 (1975).
30. Takahashi, S. and Tachiki, M., *Phys. Rev.* **B33**, 4620 (1986).
31. Aslamazov, L. G. and Larkin, A., *Phys. Lett.* **A26**, 238 (1968).
32. For a review see Skocpol, W. J. and Tinkham, M., *Rep. Prog. Phys.*, **38**, 1409 (1975).
33. Maki, K., *Prog. Theor. Phys.* **39**, 897 (1968) and *ibidem* **40**, 193 (1968).
34. Thompson, R. S., *Phys. Rev.* **B1**, 327 (1970).
35. Tachiki, M. and Takahashi, S., *Solid State Comm.* **72**, 1083 (1989).
36. Roas, B., Schultz, L. and Saemann-Ischenko, G., *Phys. Rev. Lett.* **64**, 479 (1990).
37. Clem, J. R., *Phys. Rev.* **B12**, 1742 (1975).
38. Ekin, J. W. and Clem, J. R., *Phys. Rev.* **B12**, 1753 (1975).
39. Sherrill, M. D. and Lindstrom, W. A., *Phys. Rev.* **B11**, 1125 (1975).
40. We are indebted to Prof. V. V. Moshchalkov for suggesting this graph.